Bachelorarbeit

Simulation of Electron Backscattering from an Aluminium/Hostaphan/Aluminium/PMMA Sample using PENELOPE

Atominstitut

TU Wien

Supervisors: Dipl.-Ing. Jacqueline Erhart
Dr. Gertrud Konrad
Prof. Dr. Hartmut Abele

by

Claus Kovacs

2015

Dedicated to Philippe T. Pinard for writing pyPENELOPE and answering more than two dozen of e-mails

Without his help this could never be what it is now

Abstract

PERKEO III is a spectrometer for studying the beta decay of free neutrons. For the set-up in the PERC lab of the Atominstitut, i.e., one detector vessel of PERKEO III, a new sample holder has been developed in order to facilitate measurements with calibration sources. Because of the asymmetric set-up of PERKEO III in the PERC lab and the new design of the sample holder electrons from the calibration source can be backscattered off the sample holder (initially also from PERKEO III) to the detector which is not desirable. To investigate the influence of these backscattered electrons computer simulations have been performed with the program PENELOPE. The program PENELOPE, its operation as well as the processing of its simulation results are described in this thesis. The simulations are compared with measurements. In addition, the influence of simulation parameters on the simulation results is examined.

Zusammenfassung

PERKEO III ist ein Spektrometer mit welchem der Beta-Zerfall des freien Neutrons untersucht wird. Der Versuchsaufbau im PERC Labor des Atominstituts besteht aus einer Detektoreinheit von PERKEO III. Für diesen wurde ein neuer Probenhalter entwickelt, um die Messzeiten mit Kalibrierquellen zu beschleunigen. Aufgrund des asymmetrischen Aufbaus von PERKEO III im PERC Labor und der neuen Probenhaltergeometrie können Elektronen vom Probenhalter (ursprünglich auch von PERKEO III) zum Detektor zurückgestreut werden, was nicht erwünscht ist. Um den Einfluss dieser rückgestreuten Elektronen zu untersuchen, wurden Computersimulationen mit dem Programm PENELOPE durchgeführt. Das Programm PENELOPE, seine Funktionsweise sowie die Auswertung der Simulationsergebnisse werden in dieser Arbeit beschrieben. Des weiteren werden Simulationen mit Messungen verglichen und der Einfluss von Simulationsparametern auf die Simulation untersucht.

Table of contents

1 Introduction

1.1 The Beta Decay of the Free Neutron

Bound neutrons in stable nuclei are stable. Free neutrons are unstable and undergo beta−decay with a mean lifetime of about 15 minutes [PDG15]:

$$n \rightarrow e^- + p + \bar{\nu}_e \tag{1}$$

The free neutron decays into an electron, a proton and an electron-antineutrino.

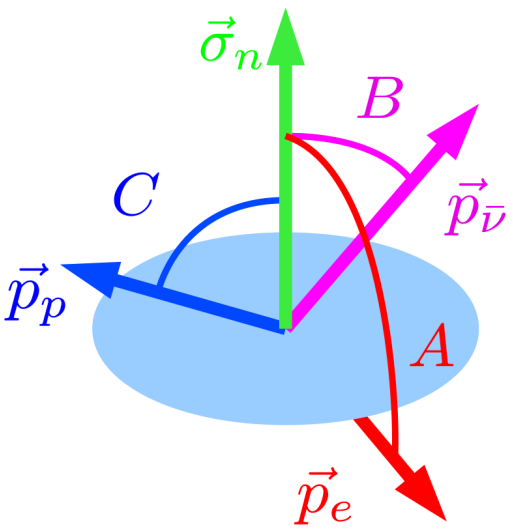

Figure 1: Neutron decay products and angular correlations [Mes11]. The momenta of the decay particles are $\vec{p}_p$ (proton), $\vec{p}_e$ (electron) and $\vec{p}_\bar{\nu}$ (electron-antineutrino).

The decay products are emitted under certain angles as shown in Fig. 1. The angular correlation coefficients (A, B and C) are measured relative to the neutron spin $\vec{\sigma}_n$.

Standard Model parameters are related to the correlation coefficients A, B and C. For example, the element V_{ud} of the CKM-matrix can be determined from the lifetime of the neutron and the electron-asymmetry parameter A. More information can be found in [Abe08].

1.2 PERKEO III: Measurement Set-up

The spectrometer PERKEO III was built 2006 in Heidelberg. It consists of a decay volume in the middle and two detector vessels to the left and the right as shown in Fig. 2a.

From one side a collimated beam of cold neutrons enters the evacuated decay volume where only a small fraction decays. The charged decay products are guided from the decay volume to the detectors through a magnetic field. This magnetic field is generated by 50 solenoids placed around the decay chamber and the two detector vessels. The remaining neutrons pass through PERKEO III and are stopped at its end by a beamstop. The main purpose of the magnetic field is to separate the charged decay products from the neutron beam and to transport the decay electrons to the detectors at both ends of the detector vessels.

Inside each of the two detector vessels a detection unit is placed, which detects the electrons from the neutron decay (see Sec. 1.2.1). Neglecting the magnetic mirror

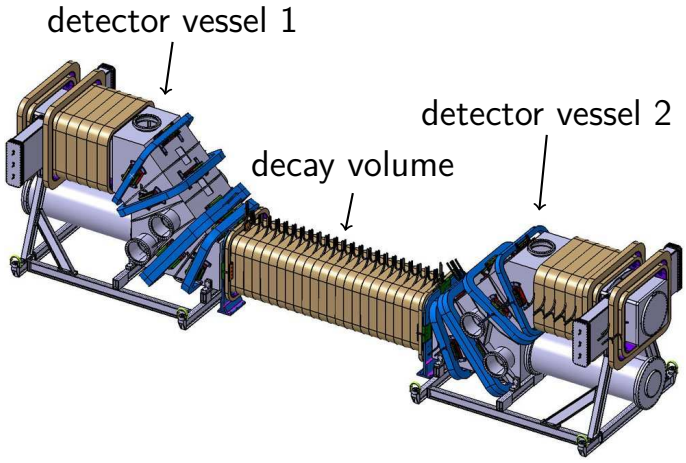

(a) Overview of PERKEO III [Mae06].

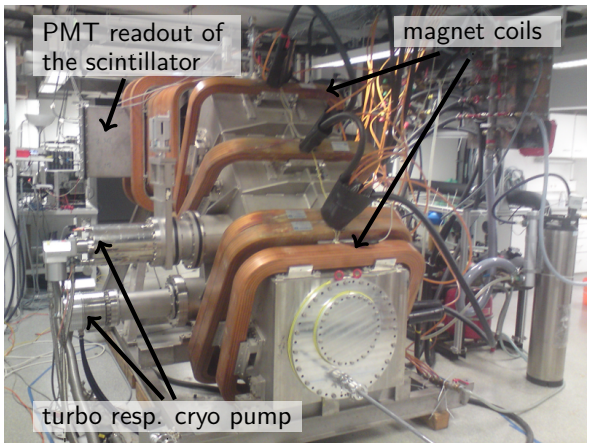

(b) View of the detector vessel in the PERC lab of the Atominstitut. More information is given in Sec. 1.2.2.

Figure 2: PERKEO III: overview and a picture of the detector vessel in the PERC lab of the Atominstitut.

effect in the decay volume, the two detectors distinguish the decay electrons with respect to the neutron spin, i.e., emitted into the same hemisphere as the neutron spin or emitted into the opposite hemisphere.

1.2.1 Detection System

Each detector vessel contains a detection unit which consists of a plastic scintillator made out of Polyvinyltoluene ($C_{10}H_{11}$) optically coupled via light guides to six photomultiplier tubes (PMTs). The housings for these units can be seen in Fig. 2.

The purpose of the plastic scintillators is to detect the kinetic energy of the decay electrons. The decay electrons hit the scintillator and generate a light flash. This light flash is guided via light guides to the PMTs.

The signals from the scintillators are amplified with the PMTs and subsequently transmitted to the outside, where the electronics system processes and the DAQ computer finally saves the measurement data. Figure 3 shows the scintillator, the light guides and the PMTs.

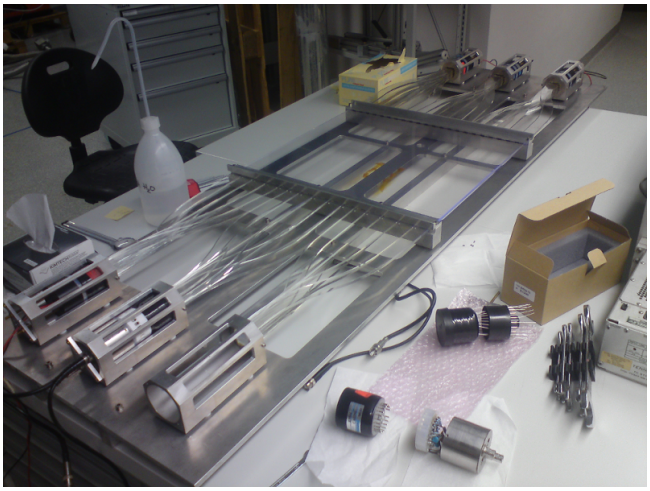

Figure 3: Scintillator, light guides and six photomultipliers of the detection unit at the Atominstitut.

As mentioned before, the neutron spin divides the space into two hemispheres: one in the direction of the neutron spin and one opposite to the neutron spin. Each detector covers one of the two hemispheres, and measures the kinetic energy of decay electrons emitted with the neutron spin and opposite to the neutron spin. From the two energy spectra, the energy-dependent beta-asymmetry $A(E_e)$ is calculated.

1.2.2 Sample Holder

To calibrate the electron detector conversion-electron calibration sources are used. These are pipetted on a sample holder. Figure 4 shows a schematic sketch of the detector vessel and the sample holder. One detector vessel was set-up at the PERC lab of the Atominstitut. The main purpose of the setup was, to improve the detection system for the high count rates expected in the successor experiment PERC [Dub08]. This can be done without the use of neutrons.

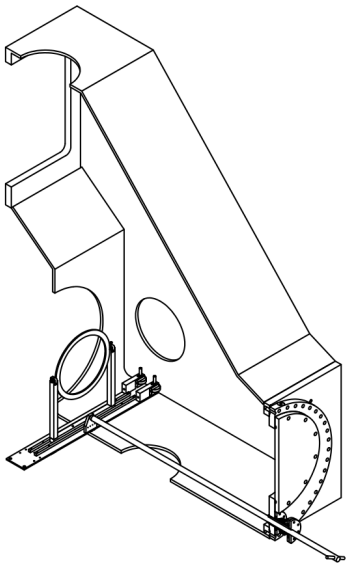

Figure 4: Cut through the detector vessel with the sample holder installed.

Inside the detector vessel, the sample holder was installed. With a rod attached to it, the holder is moved from the outside, without breaking the vacuum.

The feature to move the sample holder from the outside was quite useful. Each time breaking vacuum in order to adjust the sample holder would have been very time-consuming, because pumping out the whole vessel takes several days. With the help of the rod the sample holder is moved into the measurement position, i.e., the position in which most electrons hit the scintillator.

On the sample holder a beta emitter like ^{207}Bi is pipetted. Its Auger electrons, conversion lines or beta spectrum are used to calibrate the electron detector.

Within the scope of this thesis, a new sample holder onto which two different calibration sources can be mounted at the same time has been developed. For this purpose, two radionuclei are pipetted on the holder - one on each side. By turning the sample holder from the outside, the beta emitter facing the detector can be changed without breaking the vacuum.

1.2.3 Detector Calibration

In order to calibrate the detection system beta emitter like ^{137}Cs or ^{207}Bi are used. The radionuclei are pipetted on a thin Hostaphan ($C_{10}H_8O_4$) foil. After suitable drying time, the Hostaphan foil is screwed into the sample holder. A thin Hostaphan foil is used, in order to-originally-avoid unwanted interactions of the Auger or conversion electrons with the foil and to almost suppress energy losses of the elctrons emitted in the direction opposite to the detector, i.e., through the foil.

In order to start a (calibration) measurement, the sample holder is moved with the rod to the 'ideal' measurement position. The electronics/DAQ system 'translates' the signals from the six PMTs back into the energy (in ADC channels) deposited by the beta emitter in the plastic scintillator. At the end, we receive an energy spectrum of the radionuclei, i.e., the count rate as a function of energy in ADC channels.

The spectra of the calibration sources have either known (beta spectrum) shapes or conversion lines at known energies. By comparing the measured spectrum (energy in ADC channels) with the 'literature' spectrum for radionuclei used the detector can be energy-calibrated. Then we know which ADC channel corresponds to which energy, and the detector is calibrated.

Every calibration source has a unique shape or unique lines. By using different sources to calibrate the detection system the accuracy of the calibration can be increased.

The idea of mounting two different calibration sources at the same time on the sample holder is quite tempting. Two calibration sources can be used without breaking the vacuum - the sample holder is turned around by 180 ° and the other radionuclei is facing the detector. In this way the downtime of the experiment is drastically reduced and at the same time the efficiency of the detector calibration increased.

2 Simulation of Electron Backscattering

Once two beta emitter are mounted on the sample holder, the two calibration sources must be separated from each other, because the goal is to calibrate the detector with one source at a time. In order to separate the two sources from each other, a shielding material is placed between the two sources.

As shielding material for the sample holder acrylic glass (PMMA) has been chosen. The thickness of the shielding material is important since it should be thick enough to ideally stop all particles emitted in the direction of the detector. In order to determine the thickness needed, simulations with the program CASINO have been performed. The results are plotted in Fig. 5. For electrons with an incident energy of 1000 keV the plot shows the probability of transmission. Simulations were made for 2, 4 and 6 mm thickness. With a thickness of 6 mm almost all ($< 10^{-4}$) particles are stopped. This thickness was chosen for the sample holder.

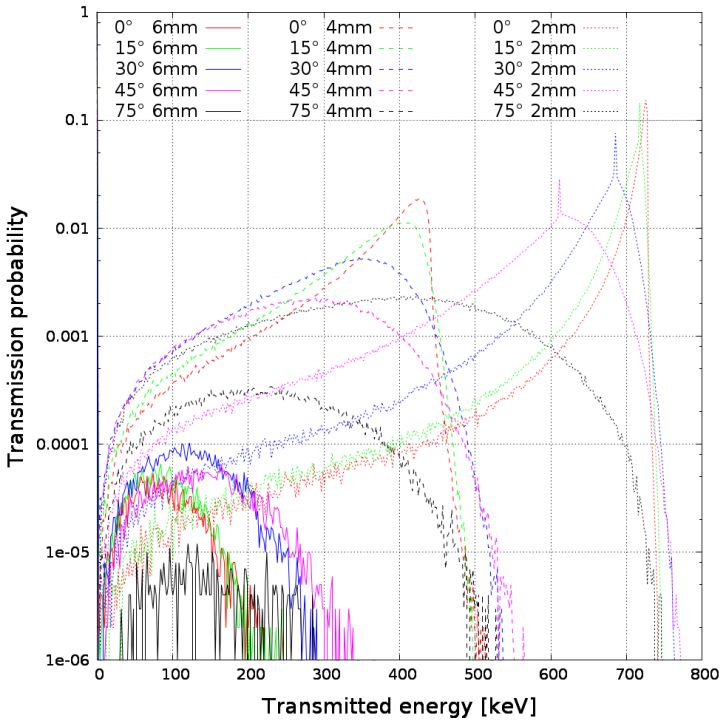

Figure 5: Probability of transmission as a function of transmitted energy for electrons with an incident energy of 1000 keV through an acrylic glass plate of thickness 2, 4 and 6 mm. The y-axis has a logarithmic scale.

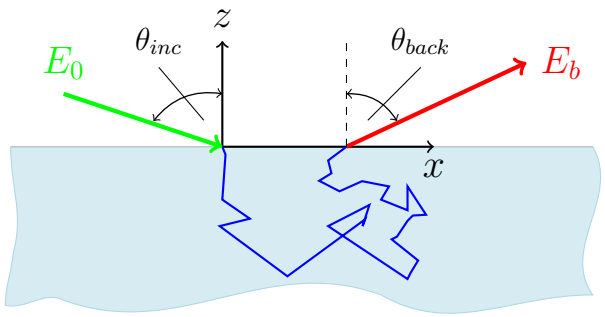

Figure 6: Example trajectory. $E_b = E_0 - \Delta E$ where ΔE represents the energy loss through collisions. The radionuclei is placed in the origin of the coordinate system and the detector in positive z-direction. A particle (green) hits the PMMA, collides and is finally backscattered (red) under an angle θ_{back} with an energy E_b.

A shielding material placed between the two radionuclei leads to a new problem: The source which is facing the detector has a 6 mm thick PMMA at its back. Electrons are emitted at all angles - towards the detector and to the rear where they hit the PMMA plate. The latter electrons might be backscattered from the PMMA and be detected. These backscattered electrons will deform the calibration spectrum, which is not desirable. In order to

calibrate the electron detector, we have to include these backscattered electrons to the 'literature' spectra. For this purpose, we have to simulate the electron backscattering from the PMMA.

In Ref. [Mos13] it was shown that CASINO is not ideally suited to investigate the backscattering of electrons from the PMMA. Therefore, we switched to PENELOPE. In this section, the program PENELOPE, its usage as well as the data processing of its output files are described.

2.1 pyPENELOPE

The program used for our simulations was PENELOPE[1] [Pen12], version 9.2.

PENELOPE is written in Fortran and prodives a Monte Carlo code with which the passage of charged particles (electrons, protons) and photons[2] through solid matter can be simulated. The energy range covered lies between 50 eV and 1 GeV. Fortunately, pyPENELOPE [Pyp12] provides a graphical user interface (GUI) for PENELOPE. pyPENELOPE, is written in Python and uses the libraries of PENELOPE. With the GUI it is easy to set up and run simulations.

Two types of simulations can be performed with pyPENELOPE:

- The first one is the PENEPMA simulation: particles impinge with an impact energy under a tilt angle θ_{tilt} on a solid surface. pyPENELOPE simulates the passage of the particles through the solid and summarizes the results at the end. Results are textfiles that contain the simulation results, for instance the backscattering probability as a function of the backscattering angle θ_{back}. During simulations the secondary electrons generated are always taken into consideration.
- The second one is called a SHOWER simulation: the possible settings are mainly the same as in the PENEPMA simulations. But the only output of a SHOWER simulation is a textfile with the name *pe-trajectories.dat* in which the trajectories and the corresponding energies of every particle are stored. During SHOWER simulations the tracking of secondary electrons is optional.

From now on, the names PENEPMA and SHOWER refer to the simulation types described above.

[1] The PENELOPE (Penetration and ENErgy LOss of Positrons and Electrons) code was integrated into GEANT4 [Gea13] in order to close the gap in low energy simulations.
[2] Here and in the following, we will speak only of (charged) particles.

2.1.1 Coordinate System

The coordinate system in the PENEPMA simulations is causing serious problems, as we will see in a moment. Figure 7b shows the coordinate system in a PENEPMA simulation: In these simulations the (solid) surface is tilted around the y-axis by the angle θ_{tilt} and the electrons always impinge in the direction of the z-axis.

With regard to the purpose of this thesis, tilting the surface gives not the correct answer. The detector (see red example detector in the pictures below) should remain in place relative to the surface. The impinging particle beam should be tilted against a fixed surface as shown in Fig. 7a. Please note that in our experiment neither the detector nor the surface of the calibration source is moving during the measurement.

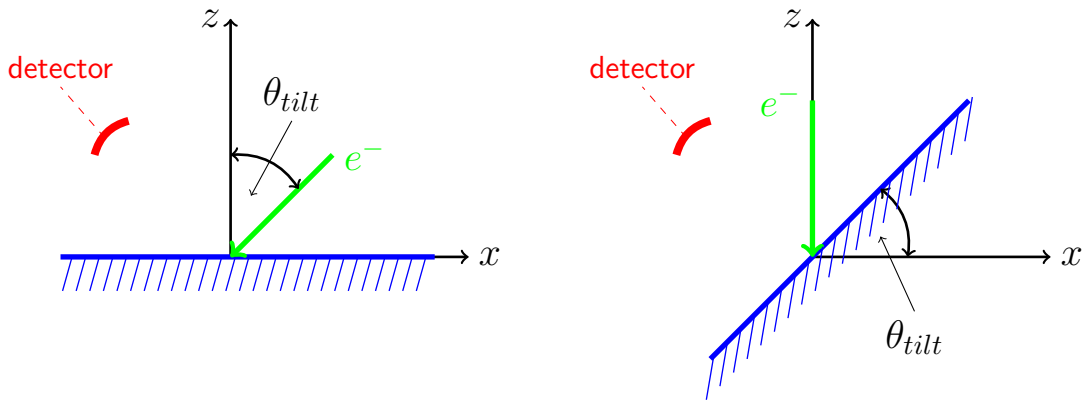

(a) SHOWER coordinate system with a detector under $\theta_{tilt} = 45\,°$.

(b) PENEPMA coordinate system with a detector under $\theta_{tilt} = 45\,°$.

Figure 7: SHOWER versus PENEPMA coordinate system.

Figure 7a shows the case we are interested in: particles impinge the (solid) surface under an angle θ_{tilt}. They can hit the surface material under a different angle θ_{tilt} but the detector does not move relative to the surface when θ_{tilt} changes.

More information about the problem in the PENEPMA simulations and its impact on the simulation results are illustrated in Figs. 9 and 17.

To summarize, the PENEPMA simulations are not suited for our application. The only way to get the simulation results we need is to extract and post-calculate then from the output file *pe-trajectories.dat*. The only use of the PENEPMA simulations is to check if our program (the extraction and post-calculation of the simulation results from the SHOWER data) works correctly (see Sec. 2.3 for details).

2.1.2 Processing of SHOWER Simulation Results

In order to extract and post-calculate the SHOWER simulation results serveral steps have to be executed:

I. Extract the exit angles and energies of the backscattered particles
II. Convert the extracted data into spherical bins
III. Process the binned data

Table 1 shows an extract of the *pe-trajectories.dat*:

		⋮				
000000000000000000000000000000000000000000000000000000000000000000000000000000000000000000000000						
TRAJ	144	number of particle (0 . . . maxparticle)				
KPAR	1	Type of particle (electron=1, photon=2, positron=3)				
PARENT	0	Index of the parent trajectory (primary=0)				
ICOL	0	Type of collision that created this trajectory (primary=0)				
EXIT	1	Exit type (backscattered=1, transmitted=2, absorbed=3)				
111111111111111111111111111111111111111111111111111111111111111111111111111111111111111111111111						
-0.144084E-07	-0.344372E-07	0.100000E+02	0.100000E+05	0.100000E+01	2	0
-0.144084E-07	-0.344372E-07	0.000000E+00	0.100000E+05	0.100000E+01	1	0
-0.144084E-07	-0.344372E-07	-0.896244E-06	0.997569E+04	0.100000E+01	1	1
0.753034E-07	-0.140091E-06	-0.221883E-05	0.997569E+04	0.100000E+01	1	5
⋮	⋮	⋮	⋮	⋮	⋮	⋮
0.314692E-06	-0.313681E-04	-0.223488E-06	0.826875E+04	0.100000E+01	1	3
0.455019E-06	-0.316395E-04	-0.595239E-07	0.821806E+04	0.100000E+01	1	1
0.330309E+36	-0.841022E+36	0.428460E+36	0.821806E+04	0.100000E+01	2	1
000000000000000000000000000000000000000000000000000000000000000000000000000000000000000000000000						
TRAJ	145					
		⋮				

Table 1: Extract of a SHOWER simulation output file (*pe-trajectories.dat*). The first three columns contain the cartesian coordinates in cm, the fourth column the corresponding energy of the particle and the remaining columns information about the surface material and the origin of the collision. For us, the first four columns are important.

This file contains all trajectories computed by a SHOWER simulation. Each trajectory starts with a line of zeros. After this line the header follows. It contains five indices which describe the trajectory like e.g. the type of particle (the descriptions are added in red in the table above). Then a line of ones follows which indicates the start of the trajectory. The particle enters the surface into the z-direction and collides inside of the surface material. During collisions it loses continuously energy. When the particle exits the surface into the positive z-direction or is absorbed inside of the surface material, the end of the trajectory is reached. It follows a line of zeros. Then the next trajectory starts.

The file size of the *pe-trajectories.dat* strongly depends on the simulation parameters.

For us, the most important simulation parameters are the following three:

- The absorption energy of electrons which is the boundary value for the energy at which the computation of the particle trajectory stops. The corresponding particles are counted as absorbed ones.
- The other two parameters are cutoff energy loss of inelastic collisions, short *WCC*, and cutoff energy loss of Bremsstrahlung emission, short *WCR*.

The file size of the output file from a SHOWER simulation is affected by these three parameters and, in addition, by the incident energy of the primary particle, the optional tracking of secondary electrons and the thickness of the surface material, which in turn may be composed of several layers of different material of different thickness. The higher the incident energy and the thicker the surface material are (up to a certain thickness at which all particles are being absorbed) the longer the particle's trajectory through the material will be, and subsequently the larger the file size will be. The optional tracking of secondary electrons increases the file size dramatically because then a lot of secondary electrons are generated and the additional information must also be stored.

The average file size for a simulation of 500.000 particles with an incident energy of 500 keV and without secondary electrons is about 30 GB. With secondary electrons enabled and stringent parameter settings the file size would grow enormously. For example a higher incident energy causes more secondary electrons: The particle starts with a higher incident energy and can therefore collide more often before reaching the energy at which it is absorbed. Therefore more secondary electrons will be generated.

For fixed storage capacity the result of simulations with tracking secondary electrons enabled may become less detailed. This is because the tracking of secondary electrons needs additional disk space. And if there is not enough space to record the secondary electrons data, other parameters like, e.g., the total amount of simulated particles must be reduced to compensate the file growth.

In order to extract and process the simulation results from the *pe-trajectories.dat* a program[3] was written. The goal was to determine the same probability and energy/angle distributions as with the PENEPMA simulations but without the incorrect tilting of the surface. As stated above the following steps must be executed for this purpose:

I. Extract the exit angles and energies of the backscattered particles

The first step is to parse the output file (*pe-trajectories.dat*) of the SHOWER simulation and to extract all data needed: the exit vectors (directions) and the backscattering energy of the simulated particles.

II. Convert the extracted data into spherical bins (binning)

After that, every exit vector is turned back by the angle $-\theta_{tilt}$. This solves the problem of the tilted surface as described in Sec. 2.1.1.

The raw data from step I contains the trajectory and energy of every backscattered particle.

Because of the finite number of simulated particles, we first have to determine into which, solid angle a particle has been backscattered. Only for an infinite number one could determine, e.g., the backscattering probability for any angle. We note that with increasing number of simulated particles the discretization of the sphere through a finite number of solid angles can be improved.

How do we implement the discretization into our analysis? We assume that the center of the sphere is the point at which the particles enter the surface. Using spherical coordinates every solid angle element then is defined by four angles. From now on we refer to a solid angle element as a bin.

Figure 8 shows an example bin for the angles $\phi_1,\ \theta_1 = 40\,^\circ$ and $\phi_2,\ \theta_2 = 70\,^\circ$. Our bins collect data. This can be for example the information that a particle passes through the solid angle. Or it may be the backscattering energy of a particle which passes the surface of the bin. This procedure is called binning.

[3]The program can be downloaded from https://github.com/clauskovacs/pypenelope-emerg-eng-ang

How is the binning implemented into our program? First of all the surface of the sphere is divided into a regular grid in terms of polar and azimuthal angle (every surface element is one bin). The program goes through all exit vectors and, if the vector passes the solid angle, the counter for the corresponding bin is incremented by one.

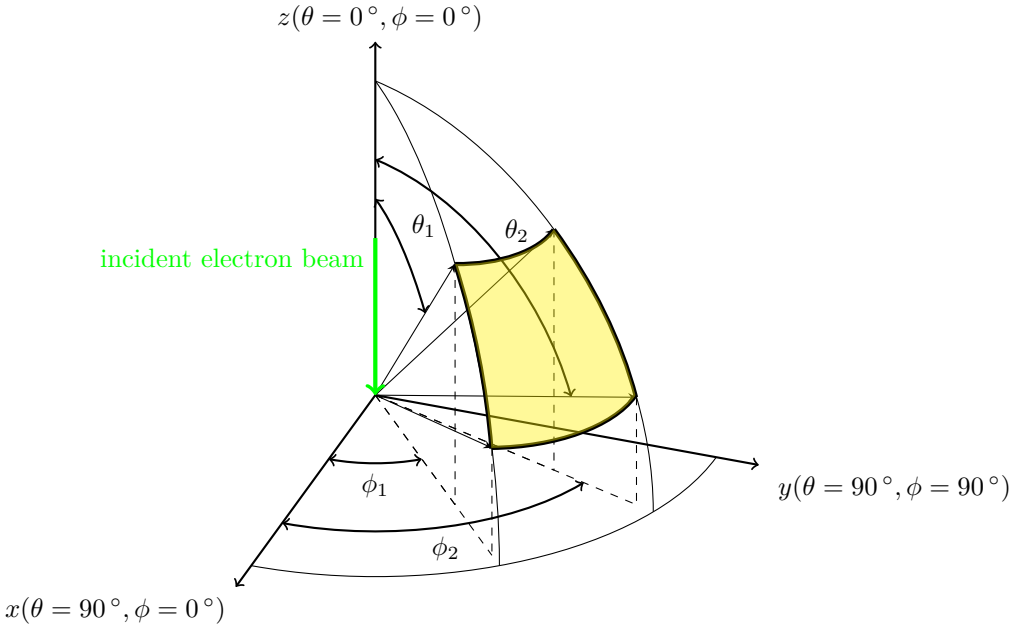

Figure 8: Example bin: $\theta, \phi \in [40\,^\circ, 70\,^\circ]$.

The amount of bins chosen and subsequently their size mainly depends on the number of simulated particles. For a constant number or incident particles there is an ideal number of bins.

From step II we receive the "probability" $\mathcal{P}(\theta, \phi)$, i.e., the amount of backscattered particles in every single bin.

III. Process the binned data

Because of the different size of the solid angle elements, we have to "normalize" the binned data from step II to the size of the bin. Therefore the data from step II is now divided by the size of the corresponding bin $\mathcal{A}(\theta, \phi)$ and the total number of simulated particles n_p:

$$\widetilde{\mathcal{P}}(\theta,\phi) = \frac{\mathcal{P}(\theta,\phi)}{n_p \cdot \mathcal{A}(\theta,\phi)} \tag{2}$$

The size of each bins is calculated as follows

$$\begin{aligned} \mathcal{A}(\theta,\phi) = \int_{\theta_1}^{\theta_2}\int_{\phi_1}^{\phi_2} sin(\theta)\, d\phi\, d\theta = \left\{ -cos(\theta)\Big|_{\theta_1}^{\theta_2} \cdot \phi\Big|_{\phi_1}^{\phi_2} \right\} = \\ = \left\{ \Big(cos(\theta_1) - cos(\theta_2)\Big) \cdot \Big(\phi_2 - \phi_1\Big) \right\} \end{aligned} \tag{3}$$

If we plot $\widetilde{\mathcal{P}}(\theta,\phi)$ as function of the angles θ and ϕ we recieve the so called backscattering clouds. A more detailed description is provided in Sec. 3.1.

Since we are not interested in the azimuthal angles ϕ, we finally integrate over ϕ. Numerically this corresponds to the sum of all bins with the same polar angle θ, i.e., for each angle θ_k all probabilities $\widetilde{\mathcal{P}}(\theta_k,\phi_i)$ for all angles ϕ_i are added up:

$$\check{\mathcal{P}}(\theta_k) = \frac{1}{n_\phi} \sum_{i=0}^{n_\phi} \widetilde{\mathcal{P}}(\theta_k,\phi_i) \tag{4}$$

Here, n_ϕ is the number of bins in terms of the azimuthal angle ϕ. A distribution $\check{\mathcal{P}}(\theta_k)$ is presented in Fig. 19 and discussed in Sec. 3.3.

Finally, we are interested in the backscattering probability as a function of backscatter energy. For this purpose, we similarly have to discretize the backscatter energy by energy bins. The energy range from zero to the incident energy E_0 was divided into a regular grid. Every element corresponds to a bin. Every backscattered particle is sorted into its corresponding energy bin, i.e., the counter of the bin which corresponds to the backscatter energy of the particle is increased by one. At the end, the binned raw data $E(b)$ is normalized:

$$\widetilde{E}(b) = \frac{E(b)}{n_p} \cdot \frac{n_e}{E_0} \qquad b = 0 \ldots n_e \tag{5}$$

The number n_e is the number of (energy)bins. A distribution $\widetilde{E}(b)$ is plotted in Fig. 18.

2.2 Problems Caused by the Coordinate System

As explained in Sec. 2.1.1 during the PENEPMA simulations the material surface is tilted and the electrons enter the surface into the negative z-direction. The resulting problem of the incorrect treatment of the angles during PENEPMA simulations is illustrated in Fig. 9b. The backscattering angle θ_{back} is always measured from the z-axis (see Fig. 6). Figure 9 shows the result of the two SHOWER respectively PENEPMA simulations [par01][4] which have been performed with the same settings. The differences between the SHOWER and the PENEPMA simulation are obvious.

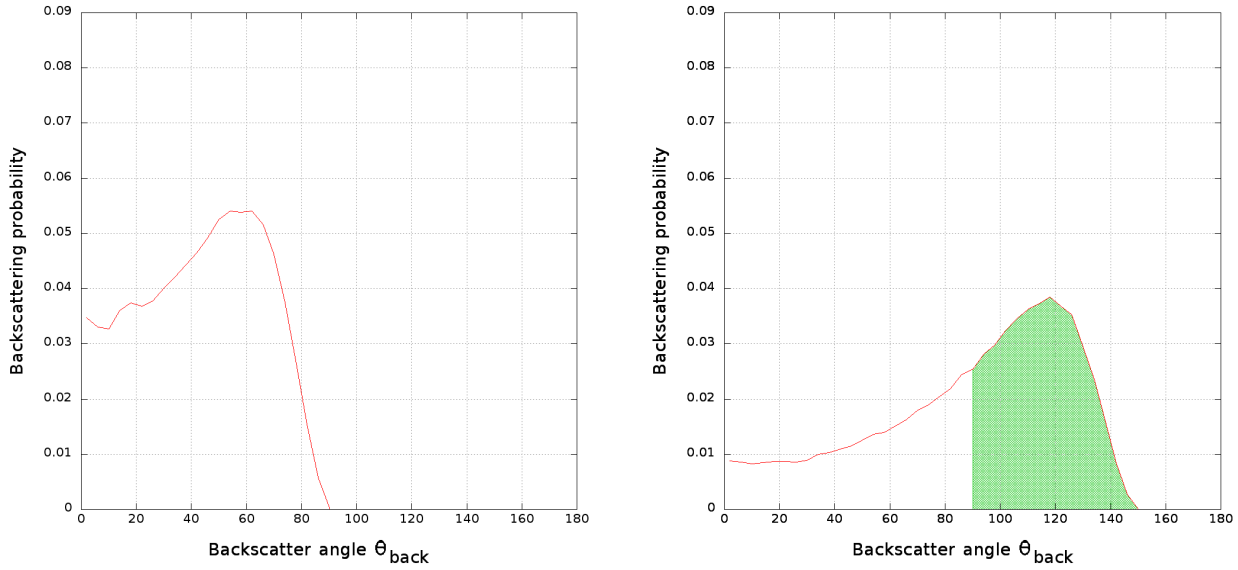

(a) SHOWER simulation

(b) PENEPMA simulation

Figure 9: Comparison between a SHOWER and a PENEPMA simulation with $\theta_{tilt} = 60\,^\circ$ [par01] (see also Footnote 4).

The backscatter angles of the PENEPMA simulation are between $0\,^\circ$ and $(90\,^\circ + \theta_{tilt})$. This is a result of the incorrect treatment of the angles. The green shaded area in Fig. 9b illustrates the problem.
There are reasons the believe that angles between $0\,^\circ$ and $90\,^\circ$ correspond to backscattered particles, while angles between $90\,^\circ$ and $180\,^\circ$ would correspond to absorbed particles. However, due to the turning of the surface by θ_{tilt}, without turning the coordinate system, angles between -$90\,^\circ$ + θ_{tilt} and $90\,^\circ$ + θ_{tilt} correspond to backscattered particles. Intuitively, one would think, that it is sufficient, to transform back the distributions by θ_{tilt}. However, in three dimensions this is not correct, since one has to transform every exit vector. Therefore we have

[4]Every single simulation has an unique ID like [par00]. The parameters for each simulation are listed in Appendix A.1.

to use the SHOWER simulations. The processed SHOWER data are presented in Fig. 9a: there are no backscattered particles between 90 ° and 180 °. Only for vertical impact ($\theta_{tilt} = 0\,°$) SHOWER and PENEPMA simulations match.

2.3 Plausibility Check

In order to validate our program to extract and process to simulation results a plausibility check has been performed. This includes comparisons between measurements and SHOWER simulations as well as between SHOWER and PENEPMA simulations.

I. Kanter

The spatial distribution of backscattered electrons from an aluminium surface has been measured by Helmut Kanter for different impact energies and angles [Kan57].

Figure 10 shows one measurement done by Kanter. Electrons with an energy of 10 keV (or 50 keV) enter an aluminium substrate under an angle γ. The energy of the backscattered particles was presented in a polar plot. The polar axis is in units of the incident energy.

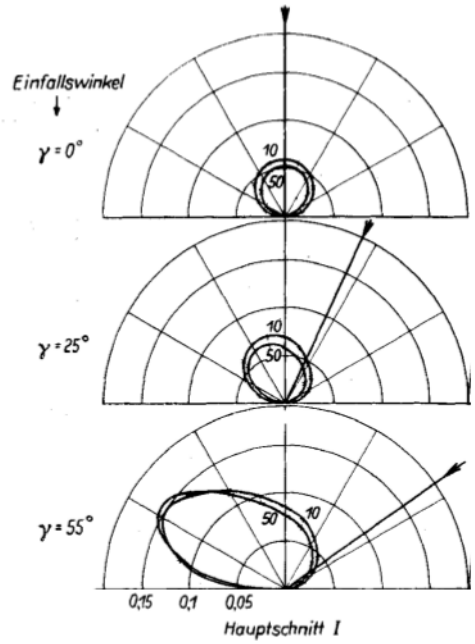

Figure 10: Measurement of backscattering by Kanter [Kan57]. Incident energy $E_0 = 10\,\text{keV}$ (or 50 keV), incident angles $\gamma = 0\,°, 25\,°, 55\,°$.

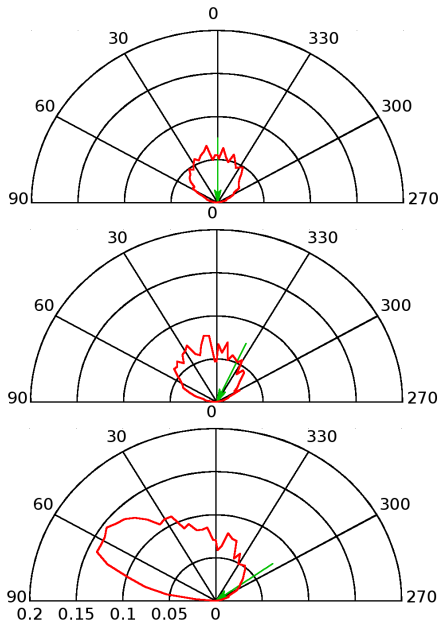

Figure 11: SHOWER simulations comparative to the measurements by Kanter (see Fig. 10 for details) [par02].

A comparative simulation [par02] of electrons with an energy of 10 keV and the same angles γ impinging an aluminium surface has been performed in order to check if the SHOWER simulation is in agreement with Kanter's measurement.

Figure 11 shows the results of the SHOWER simulations. The figure shows the plane of the backscattering cloud in which the particles enter the surface.

The results of the SHOWER simulations are consistent with the measurements from Kanter.

II. SHOWER versus PENEPMA simulations

The next step was to examine whether the SHOWER and the PENEPMA simulations get the same results. For this purpose, the backscattering probability as a function of the backscatter energy and angle has been investigated.

Figure 12a shows the relative difference between a SHOWER and a PENEPMA simulation as a function of the backscatter angle θ_{back}.

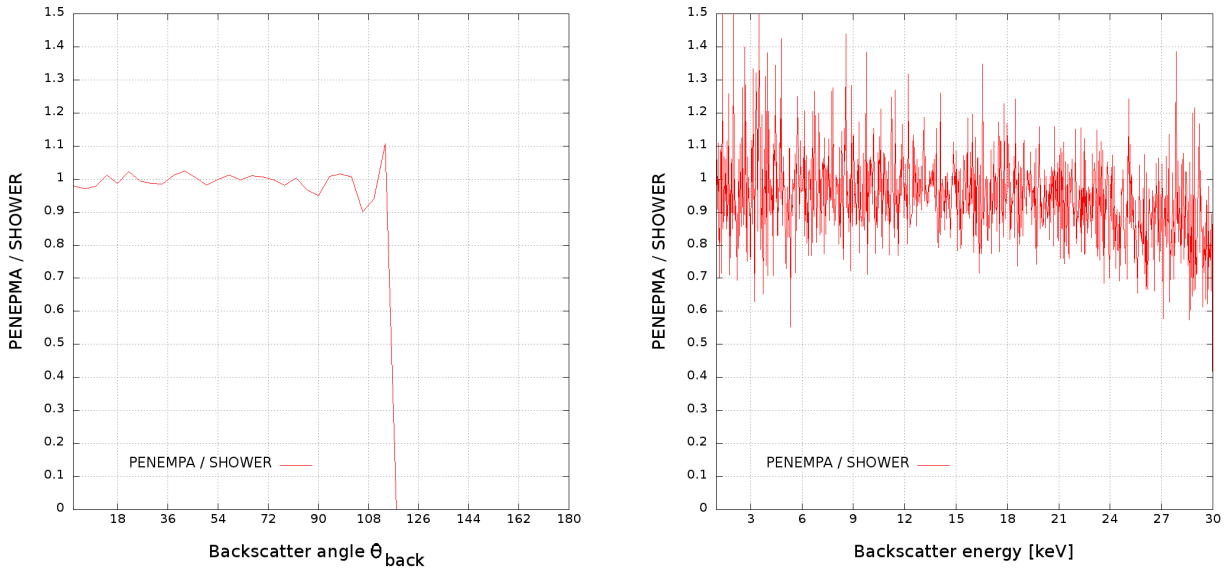

(a) Relative difference between a SHOWER and a PENEPMA simulation versus backscatter angle for $\theta_{tilt} = 25\,°$.

(b) Relative difference between a SHOWER and a PENEPMA simulation versus backscatter energy for $\theta_{tilt} = 25\,°$.

Figure 12: Comparison between SHOWER and PENEPMA simulations [par03] [par04].

The second Fig. 12b shows the relative difference between a SHOWER and a PENEPMA simulation as a function of the backscatter energy. More information about the graphs is given in Sec. 3.3.

As can been seen from Fig. 12, after the same "incorrect" treatment of the angles, SHOWER data result in the same results as the PENEPMA simulations.

2.4 Influence of Simulation Parameters

As mentioned before in Sec. 2.1.2 several simulation parameters affect the accuracy of the SHOWER simulations. One of these parameters is the cutoff parameter for the absorption energy of electrons: If a simulated particle reaches this energy due to collisions, the tracing stops and the particle is counted as an absorbed one. By default this parameter is set to one percent of the incident energy. According to the manual this should be optimal for most simulations.

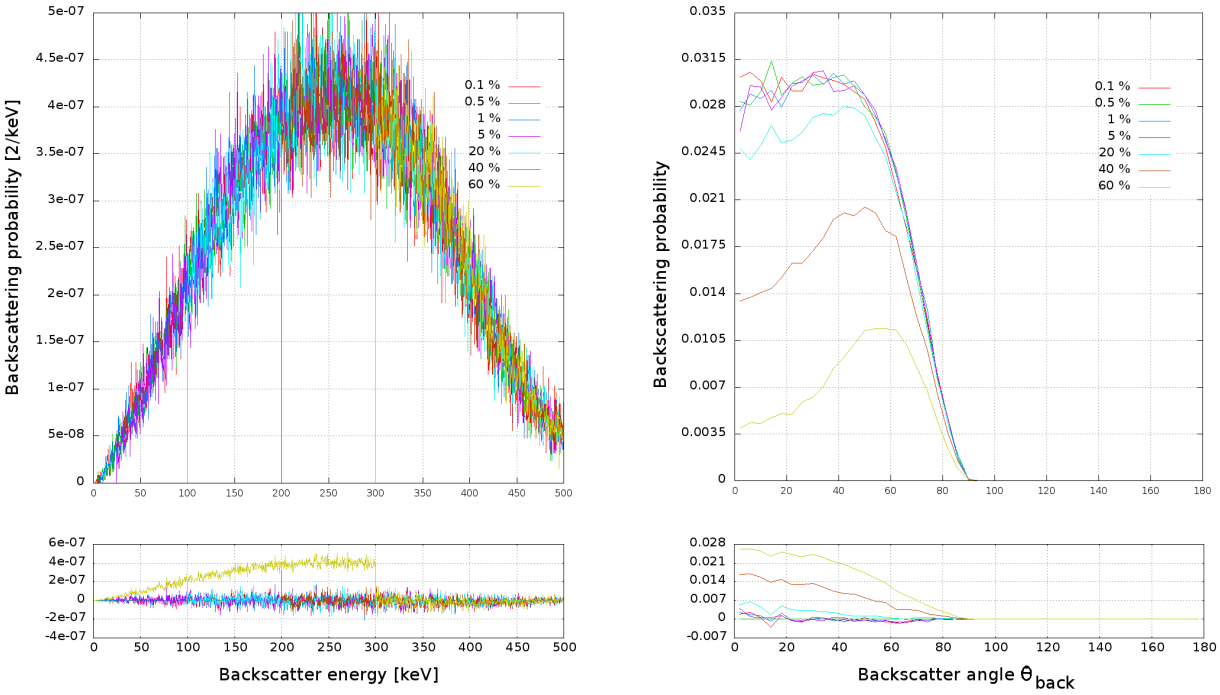

(a) Backscattering probability versus backscatter energy.

(b) Backscattering probability versus backscatter angle θ_{back}.

Figure 13: Influence of the cutoff parameter on the simulation results for $\theta_{tilt} = 45\,^\circ$ on a PMMA surface [par05]. Below the backscattering distributions the residuals of the distributions compared to the simulation with cutoff parameter equal to 0.1 % of the incident energy are shown.

Figure 13 shows two SHOWER simulations for different cutoff parameters: Here the cutoff parameter is given in percent of the initial energy.

Fazit: Use cutoff parameter smaller than 5 % because for cutoff parameters larger than 5 % there is a loss of information as can be seen from Fig. 13a: More and more particles are not registered as backscattered ones because the tracking is stopped before they could exit the surface. Therefore the backscattering probability decreases with increasing cutoff parameter.

The influence of the cutoff parameter on the time a simulation needs to run and the size of the output file is shown in Fig. 14.

With increasing cutoff parameter the output file size and the simulation time decrease because the simulation of the trajectories is stopped earlier. Both the simulation time and the file size decrease at the same speed as can be seen from Fig. 14.

With the cutoff parameter set to 1 % of the initial energy the maximum accuracy can be achieved without loss of information.

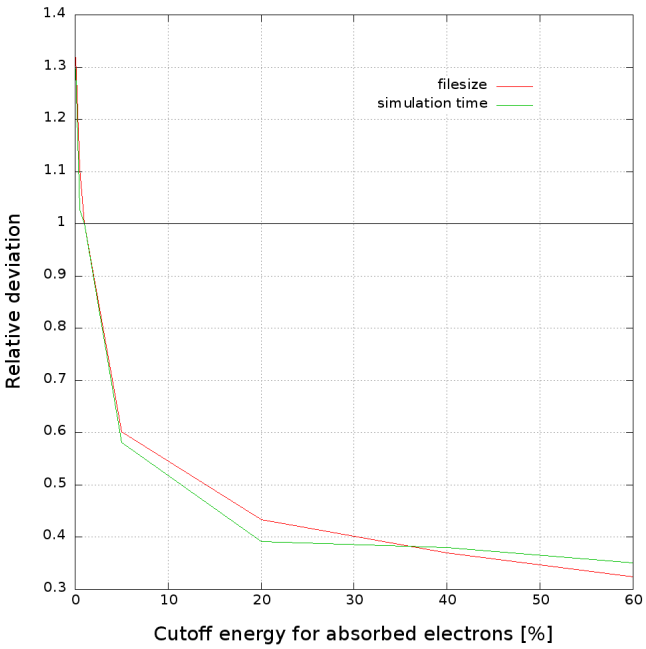

Figure 14: Influence of the cutoff parameter on the simulation time and the output file size. The cutoff energy is given in percent of the incident energy. A value of 20 % means that the cutoff parameter for the absorption energy of electrons is set to 20 % of the incident energy. The relative deviation of the simulation time and of the output file size is given relative to the simulation with cutoff parameter set to 1 % (black horizontal line).

3 Simulation Results

In Sec. 2.3 above we have pointed out that the SHOWER simulations match with measurements [Kan57]. In this section the simulation results are presented: The first part deals with backscattering clouds. These figures show how many particles are backscattered into specific solid angles.

In the second part the backscattering, absorption and transmission coefficients from the SHOWER and PENEPMA simulations are discussed.

In the last part of this section the most interesting simulation results are presented: The backscattering probability as a function of the backscatter angle θ_{back} and the backscattering probability as a function the backscatter energy. These two distributions are exactly what is needed for the correction of electron backscattering in PERKEO III.

As introduced in Sec. 2 the surface material examined in these simulations is a stack of 40 nm Al, 25.000 μm Hostaphan, 40 nm Al and 6 mm PMMA ($C_5H_8O_2$) as shown in the Fig. 15 below. In order to prevent a potential charging of the sample holder, we used a laminated Hostaphan foil. In the simulation this is realized with a thin layer of aluminium on each side of the Hostaphan foil.

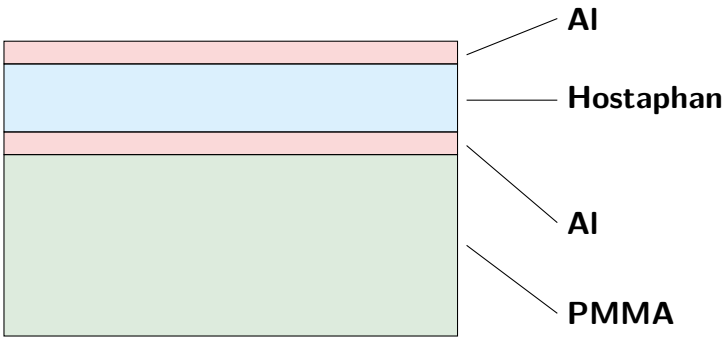

Figure 15: Surface material of our sample holder (see text for details).

In the SHOWER simulations the particles enter the sample holder from the top of the surface.

3.1 Backscattering Clouds

Processing of the SHOWER simulation data (for details see Sec. 2.1.2) results in the so called backscattering clouds. These are a graphical representation of the backscattering probability into a given solid angle element.

Figure 16 shows two backscattering clouds for an incident electron energy of 500 keV but two different incident angles. The vector $\vec{v}_{inc}$ under which the electrons enter the surface always lies in the x-z-plane and is rotated around the y-axis by the incident angle θ_{inc}.

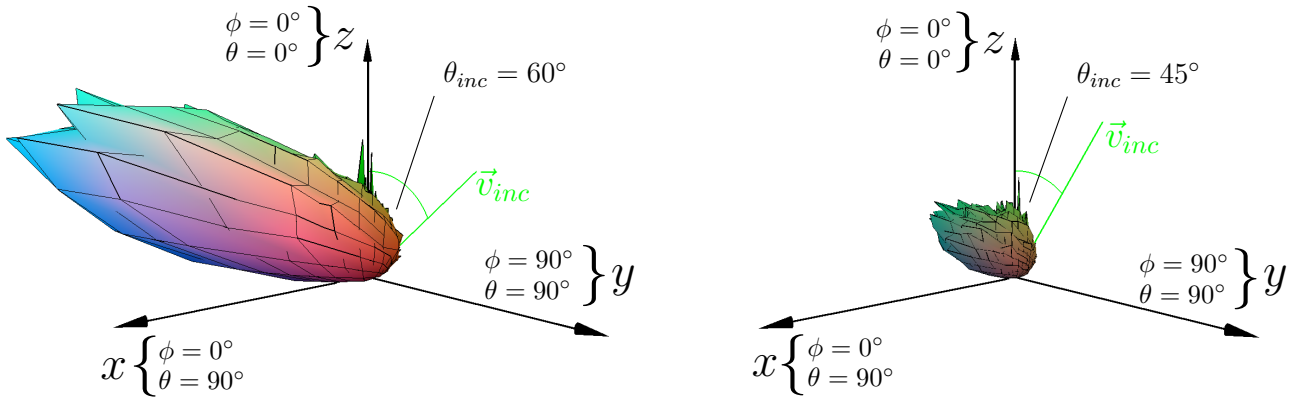

(a) Incident angle $\theta_{inc} = 60°$

(b) Incident angle $\theta_{inc} = 45°$

Figure 16: Backscattering clouds for an incident energy of 500 keV and $\theta_{inc} = 45\,°$ and $60\,°$ [par06].

In both figures 16 above the axis have the same length. It is obvious that for a larger angle θ_{inc} the backscattering probability is higher and therefore the cloud becomes larger.

We note that the x-z-plane is a mirror plane of all backscattering clouds as the incident vector $\vec{v}_{inc} = (x\ 0\ z)^T$ lies in this plane.

We further note that the main purpose of this visualization is to check whether our program performs correctly.

3.2 Backscattering-, Absorption- and Transmission Coefficients

For any SHOWER or PENEPMA simulation the total number of backscattered, transmitted and absorbed particles can be easily obtained. By dividing these numbers by the total number of simulated particles the corresponding coefficients are calculated (e.g., the backscattering coefficient is the number of backscattered particles divided by the total number of simulated particles).

Figure 17a shows the coefficients from a SHOWER simulation as a function of the incident angle. For vertical incidence fewest particles are backscattered. With increasing incident angle, more particles are backscattered. For higher incident energies the backscattering coefficient slightly decreases. We note that the sum of backscattered, transmitted and absorbed particles gives always one because of the conservation of the total number of simulated particles.

The coefficients presented in Fig. 17a are consistent with simulations from other groups [Wie04].

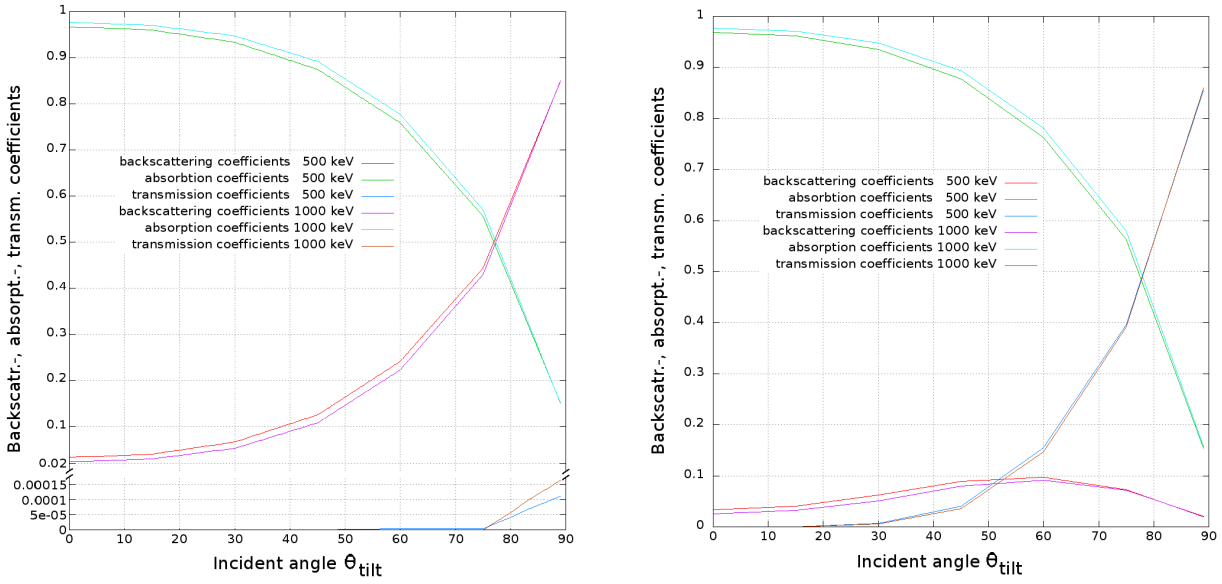

(a) Backscattering, absorption, and transmission coefficients of SHOWER simulations.

(b) Backscattering, absorption, and transmission coefficients of PENEPMA simulations.

Figure 17: Backscattering, absorption and transmission coefficients of SHOWER [par07] and PENEPMA [par08] simulations. The values of all simulation parameters are listed in Appendix A.2.

Figure 17b shows the coefficients obtained from a PENEPMA simulation. Compared to Fig. 17a these graphs look quite strange even though. Both simulations presented in Fig. 17 have been done with the same settings. The incorrect treat-

ment of angles in the PENEPMA simulations leads to unphysical coefficients. Consequently the coefficients from the PENEPMA simulations are not correct and therefore cannot match with other simulations [Wie04].

3.3 Backscattering Probability

All simulations discussed in this paragraph have been done with the same surface material (see Fig. 15).

I. Backscattering probability as a function of backscatter energy

Figure 18 shows the backscattering probability distribution as a function of the backscatter energy, i.e., the graphs illustrate how high the backscattering probability at a certain energy of a backscattered particle is. The simulations have been performed with incident energies of 500 keV (a) and 1000 keV (b). The angle θ_{tilt} under which the electrons enter the surface was varied in 15 ° steps between 0 ° and 75 °. Figure 18a shows the simulations for a constant incident energy of 500 keV. Compared to "small" angles, the backscattering probability for $\theta_{tilt} = 75\,^{\circ}$ shows a pronounced maximum for high incident energies. In addition, the larger the incident angle θ_{tilt}, the higher the backscattering probability. At larger angles θ_{tilt} the particles lose less energy when passing through the material because they are backscattered off from the material earlier.

The simulation results presented in Fig. 18b have been conducted for 1000 keV. Compared to Fig. 18a the backscattering probability (per eV) for 1000 keV is nearly twice as high as for 500 keV, but only nearly. Note the different scaling of both axis. Hence, one cannot just multiply the probability for 500 keV with, e.g., a factor of two in order to dertermine the probability for 1000 keV. The reason for this is that for higher incident energy the particles penetrate more deeply into the surface material. For 1000 keV therefore a little more particles are absorbed than backscattered because they reach deeper depths.

The backscattering coefficients for different incident energies but same incident angles are almost identical as can be seen from the comparision of Tables 2 and 3 in Appendix A.2 This is not obvious from Fig. 18 due to the different scaling of both axis. Note that the almost energy independence of the backscattering coefficients can also be seen from Fig. 17a. To verify the consistency of the simulation results, the backscattering coefficients have additionally been calculated by integration of the simulation data presented in Fig. 18 using the trapezoidal

rule. The resulting values are listed in Appendix A.3, and are in agreement with the backscattering coefficients listed in Appendix A.2.

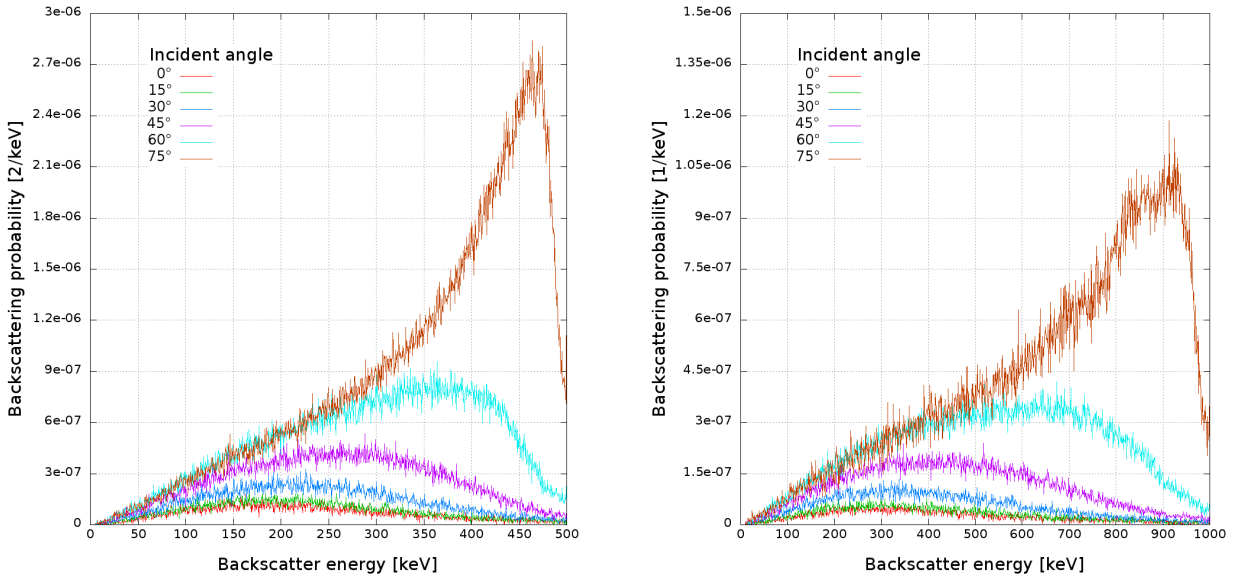

(a) Backscattering probability versus backscatter energy for incident energy 500 keV.

(b) Backscattering probability versus backscatter energy for incident energy 1000 keV.

Figure 18: Backscattering probability versus backscatter energy for incident energies 500 and 1000 keV [par09]. Please note the different scaling of both axis.

Obviously we cannot predict the simulation results for other incident energies from one simulation for a certain incident energy. Only for small changes in the incident energy the backscattering probability changes linearly.

II. Backscattering probability as a function of backscattering angle

Figures 19a and 19b show the backscattering probability as a function of the backscatter angle θ_{back} for the same settings as above: incident energies of 500 keV and 1000 keV and angles between 0 ° and 75 ° in 15 ° steps.

From these graphs the backscattering probability at a certain angle can be determined. The larger the incident angle θ_{tilt}, the higher the backscattering probability. With increasing incident angle the maximum of the backscatter distributions is moved to larger angles θ_{back}, similarly to Fig. 18.

For equal incident angle θ_{tilt} the backscattering probability distributions for 500 keV and 1000 keV are nearly the same. This means that the backscattering probability is not strongly depending on the incident energy.

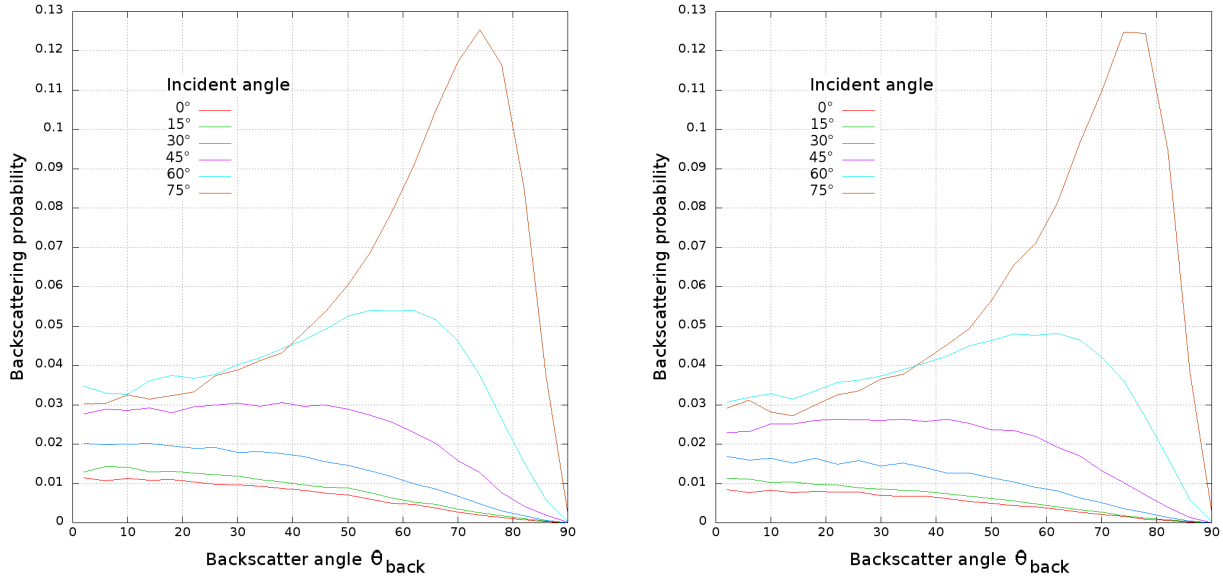

(a) Backscattering probability versus backscatter angle θ_{back} for incident energy 500 keV.

(b) Backscattering probability versus backscatter angle θ_{back} for incident energy 1000 keV.

Figure 19: Backscattering probability as a function of backscatter angle θ_{back} for incident energies of 500 and 1000 keV [par09].

4 Summary and Outlook

The main achievement of this thesis is, that there is no evidence for a deviation of PENELOPE simulations from measured data on the level of accuracy. The SHOWER simulations are in agreement with measurements of Kanter (Sec. 2.3) but should be treated carefully. Other comparisons [Mar03] show a deviation of up to 10 % between measurements and Penelope simulations.

The backscattering, absorption and transmission coefficients match those from backscattering simulations of other groups (Sec. 3.2). It has also been pointed out that the PENEPMA simulations are not suited for our problem (Secs. 2.1.1 and 2.2).

Moreover the SHOWER simulation data from the processed SHOWER simulations can be used to investigate the impact of electron backscattering in PERKEO III. For more information see [Erh16].

Potential Improvements

There is always room for improvement in the simulation of physical phenomena. The accurateness of a simulation depends on many factors. A main factor is the number of simulated particles. Here, this parameter could only be increased until the SHOWER output file took all physical storage place available. One way to solve this problem would be to modify the pyPENELOPE code in such a way that the file size of the output files is drastically reduced, e.g., by only saving the exit angles and energies of the particles. Simulations with more particles, lower cutoff parameters and secondary electrons enabled could be done without much more disk space!

The influence of secondary electrons is an interesting point that should be investigated in the future, especially if one is interested in the energy distribution of backscattered electrons at low energies. Tracking of secondary electrons during a simulation increases the simulation time and the resulting output file size dramatically and was therefore disabled in most of the simulations.

Another point of improvement is the step size of the incident angle under which the particles enter the surface: Simulations have been done every $15\,^\circ$ starting from $0\,^\circ$. If we are interested for example in the backscattering of particles entering the surface under an angle of $20\,^\circ$ we have no data available. Therefore, we would have to interpolate the results for $15\,^\circ$ and $30\,^\circ$. Interpolation errors could be reduced by reducing the step size of the incident angle.

Table of Figures

Appendix

A Tables

A.1 Simulation Parameters

The table below lists all simulations presented in this thesis together with their main parameters. For all simulations the beam diameter was fixed to 10 nm. The parameters *C1*, *C2*, *WCC* and *WCR* have always been set to default and are therefore not listed.

Sim.	Mat.	# e^-	θ_{tilt}	Incident E.	SE	Page
01	AHAP	500.000	50 °	500 keV	N	13
02	Al Subs.	1.000.000	0 °, 25 °, 55 °	10 keV	Y	14
03	Al Subs.	1.000.000	25 °	10 keV	Y	15
04	C Subs.	1.000.000	25 °	30 keV	Y	15
05	AHAP	500.000	45 °	500 keV	N	16
06	AHAP	500.000	45 °, 60°	500 keV	N	19
07	AHAP	500.000	0 ° ... 89 °	500, 1000 keV	N	20
08	AHAP	500.000	0° ... 89 °	500, 1000 keV	Y	20
09	AHAP	500.000	0 ° ... 75 °	500, 1000 keV	N	22, 23

Sim.	...	Number of the simulation
Mat.	...	Surface material used ("Subs." = substrate; "AHAP[5]" - see Fig. 15)
# e^-	...	Total number of tracked electrons
θ_{tilt}	...	Tilt angle - see Fig. 6
Incident E.	...	Incident energy of the electrons
SE	...	Secondary electrons considered during the simulation?
Page	...	Page at which the simulation can be found in this thesis

For simulation no. 5 the cutoff parameter for the absorption energy of electrons has been varied between 0.1, 0.5, 1, 5, 20, 40 and 60 % of the incident energy (see Sec. 2.4). For all other simulations this cutoff parameter was set to default, i.e., 1 % of the incident energy.

θ_{tilt} = "0 ° ... 89 °" means that the angle θ_{tilt} was set to 0, 15, 30, 45, 60, 75 and 89 °. Similar for θ_{tilt} = "0 ° ... 75 °" where the angle was set to 0, 15, 30, 45, 60 and 75 °.

[5] **A**luminium, **H**ostaphan, **A**luminium, **P**MMA

A.2 Backscattering, Absorption, and Transmission Coefficients (Sec. 3.2)

Angle	Backscattering coefficient	Absorption coefficient	Transmission coefficient
0 °	0.032	0.968	0
15 °	0.0391	0.961	0
30 °	0.0658	0.934	0
45 °	0.1255	0.875	0
60 °	0.241	0.759	0.000004
75 °	0.4428	0.557	0.000004
89 °	0.85	0.1499	0.000112

Table 2: Backscattering, absorption and transmission coefficients for electrons on our sample holder (Fig. 15) with an incident energy of 500 keV, number of simulated particles = 500.000.

Angle	Backscattering coefficient	Absorption coefficient	Transmission coefficient
0 °	0.024	0.976	0
15 °	0.0292	0.971	0
30 °	0.052	0.948	0
45 °	0.1074	0.893	0
60 °	0.2220	0.778	0
75 °	0.4292	0.571	0
89 °	0.850	0.1495	0.00016

Table 3: Backscattering, absorption and transmission coefficients for electrons on our sample holder (Fig. 15) with an incident energy of 1000 keV, number of simulated particles = 500.000.

A.3 Backscattering Coefficients (Trapezoidal Rule - Sec. 3.3)

Angle	500 keV	1000 keV
0 °	0.03195	0.02367
15 °	0.03907	0.02922
30 °	0.06575	0.05196
45 °	0.1255	0.10739
60 °	0.2409	0.22193
75 °	0.4424	0.42896

Table 4: Backscattering coefficients calculated by integration using the trapezoidal rule.

Bibliography

[Abe08] H. Abele, The neutron. Its properties and basic interactions, Prog. Part. Nucl. Phys **60**, 1-81, 2008

[Dei05] M. Deissenroth, Optimization and Realization of a Neutrino Asymmetry Measurement in the Decay of Polarized Neutrons, diploma thesis, Universität Heidelberg, 2005

[Dub08] D. Dubbers et al., A clean, bright, and versatile source of neutron decay products, NIMA 596 (2008) 238

[Erh16] J. Erhart, Energy and Momentum Spectroscopy for PERC and Searches for Time-Varying Constants, PhD thesis, TU Wien, in progress, 2016

[Gea13] Geant4 - a toolkit for the simulation of the passage of particles through matter, http://geant4.web.cern.ch/geant4/, 2013

[Kan57] H. Kanter, Annalen der Physik **20**, 144, 1957

[Mae06] B. Märkisch, Das Spektrometer PERKEO III und der Zerfall des freien Neutrons, PhD thesis, Universität Heidelberg, 2006, http://www.physi.uni-heidelberg.de/Publications/phd_maerkisch.pdf

[Mar03] J. W. Martin et al., Phys. Rev. C **68**, 2003

[Mes11] H. Mest, Measurement of the β -Asymmetry in the Decay of Free Polarized Neutrons with the Spectrometer PERKEO III, PhD thesis, Universität Heidelberg, 2011, http://archiv.ub.uniheidelberg.de/volltextserver/12198/1/dissertation_mest.pdf

[Mos13] M. Moser, Optimierung und Charakterisierung eines PERKEO III Detektors zur Elektronen-Energie-Spektroskopie, Master's thesis, TU Wien, 2013

[Pen12] PENELOPE2011, A Code System for Monte-Carlo Simulation of Electron and Photon Transport http://www.oecd-nea.org/tools/abstract/detail/nea-1525, 2012

[PDG15] K.A. Olive et al. (Particle Data Group), Chin. Phys. C **38** (2014) 090001 and 2015 partial update

[Pyp12] pyPENELOPE, GUI for the program PENELOPE2011 http://pypenelope.sourceforge.net/, 2012

[Wie04] F.E. Wietfeldt et al., A backscatter-suppressed beta spectrometer for neutron decay studies, NIMA 538 (2005) 574